Muñoz-Noval, A., Fin, S., Salas-Colera, E., Bisero, D., & Ranchal, R. (2018). The role of surface to bulk ratio on the development of magnetic anisotropy in high Ga content Fe100-xGax thin films. *In Journal of Alloys and Compounds, 745*, 413–420

DOI:10.1016/j.jallcom.2018.02.223

The role of surface to bulk ratio on the development of magnetic anisotropy in high Ga content $Fe_{100-x}Ga_x$ thin films

A. Muñoz-Noval[1,2], S. Fin[3], E. Salas-Colera[4], D. Bisero[5], and R. Ranchal[2]

[1]*Department of Applied Chemistry, Hiroshima University, Higashi-hiroshima, Hiroshima 739-8527, Hiroshima, Japan.*

[2]*Dpto. Física de Materiales, Facultad de Ciencias Físicas. Universidad Complutense de Madrid. Ciudad Universitaria s/n, Madrid 28040, Spain.*

[3]*Dipartimento di Fisica, Università di Ferrara, Via Saragat 1, 44122 Ferrara, Italy*

[4]*BM25-Spline, the Spanish CRG at the ESRF (Grenoble, France) and Instituto de Ciencia de Materiales de Madrid-CSIC (Madrid, Spain).*

[5]*CNISM and Dipartimento di Fisica, Università di Ferrara, Via Saragat 1, 44122 Ferrara, Italy*

Abstract

In this work we show the development of bulk in-plane magnetic anisotropy in high Ga-content (Ga = 28 at. %) $Fe_{100-x}Ga_x$ thin films as the layer thickness increases. This result is in clear contrast with the generally reported decrease of this anisotropy with the film thickness. We propose the interrelation between the enhancement of the Ga-pair correlations and a collinear distortion of the bcc structure within the sample plane as the origin of the magnetic anisotropy. Our results have been obtained by employing a combination of long and local range structural probe techniques with bulk and surface magnetic characterization techniques. The key point shown in this work is that the in-plane structural anisotropy and hence, the magnetic anisotropy, are developed as the layer thickness increases. This fact strongly suggests that the surface to bulk free energy ratio plays a key role in the formation of ordered phases with a distorted bcc cell in $Fe_{100-x}Ga_x$ films with *x* around 28 at. %. Our work also shows the arising of new phenomena in these high Ga content alloys due to the close correlation between structural and magnetic properties.

1. Introduction

Magnetic layers exhibit a close correlation between structural and magnetic properties [1-2] that makes possible to tailor magnetism by means of a structural engineering, e.g. by tuning growth conditions [3-4]. In the last years, $Fe_{100-x}Ga_x$ alloys have received great attention due to their unique magnetoelastic properties [5-17]. These alloys are even more versatile than other higher magnetostrictive materials as Terfenol-D, because of their better mechanical performance and chemical stability [6, 9]. The strong correlation between composition and magnetic properties in bulk $Fe_{100-x}Ga_x$ alloys is evidenced by the existence of two maxima of the magnetostriction constant (λ) for Ga contents of about 18 and 28 at.%. These maxima can be shifted to slightly higher Ga contents when using fast cooling rates during processing [12]. There is a large list of studies about the relationship between local structure and magnetic properties in Fe-based compounds such as rare earths-Fe and Fe-Ga [18-21]. Pascarelli and co-workers were pioneers in measuring the magnetostriction at atomic scale by means of dispersive X-ray absorption fine structure spectroscopy in Fe-Ga ribbons [8]. Most of the works about $Fe_{100-x}Ga_x$ investigate alloys with $x \leq 20$ at. % [5-8, 13-14, 17], although higher λ values at the second peak have been reported [12, 22-23]. This can probably be because the underlying mechanisms causing this second peak are not well understood. For example, Cao et al [9] observed evidences of nanoscale ordered precipitates in $Fe_{100-x}Ga_x$ with x up to 25 at. %. They argued that Ga can be orderly placed in the Fe matrix distorting the original bcc-Fe to a tetragonal local symmetry. This transformation would not only increase the structural anisotropy, but also alter the magnetostriction as confirmed in bulk systems [9]. Additionally, it is of particular relevance that the Ga alignment in form of Ga-pairs along the perpendicular direction to the sample plane, i.e. the [001] direction of the bcc cell (B2-like ordering), can promote perpendicular magnetic anisotropy in <100> $Fe_{100-x}Ga_x$ thin films around the first peak of magnetostriction [17].

$Fe_{100-x}Ga_x$ is a very interesting family of alloys from the technological point of view due to their high magnetostriction coefficient [11]. This property can be exploited in the recently proposed strain-controlled magnetostrictive nanodevices [24-25]. However up to now, the relationship between magnetostriction and parameters such as growth conditions or thickness are starting to be studied. In the former case, we showed that in layers around the second peak grown in different sputtering regimes, the in-plane magnetic anisotropy (IPMA) was attributed to a preferential formation of ordered

$B2/D0_3$ phases when using the ballistic regime [3]. In the latter, it is crucial to understand how the magnetic properties are modified upon the reduction of dimensionality in order to integrate $Fe_{100-x}Ga_x$ alloys in devices.

Here, we report on the development of an uniaxial IPMA as the thickness of sputtered $Fe_{72}Ga_{28}$ layers increases. The appearance of this magnetic anisotropy seems to be related to the structural anisotropy locally observed by polarization-dependent XAFS. Comparing the sample plane with its perpendicular direction we have found a cell distortion of the cubic bcc structure. In addition, experimental results indicate that two correlated effects interplay on the development of the IPMA: i) a higher and more ordered segregation of B2 phase, and ii) the preferential alignment of Ga-pairs along the sputtering direction that sets the anisotropy axis. The results indicate that the Ga-pairs that naturally appear in the B2 phase in the studied Ga content cause the cell distortion and promote the appearance of the IPMA. In the studied samples, the Ga-pairs are ordered in the substrate plane along the sputtering beam direction. This uniaxial IPMA only occurs above certain thicknesses in sputtered $Fe_{72}Ga_{28}$ layers meaning that for the studied composition, the surface to volume energy ratio of the system plays a role on the development of magnetic anisotropy.

2. Experimental section

$Fe_{72}Ga_{28}$ thin films were grown by DC magnetron sputtering from a $Fe_{72}Ga_{28}$ target at room temperature on glass substrates. The deposition was carried out in oblique incidence with an angle between the vapor beam and the perpendicular to the sample of about 25°. The layers were deposited with a growth power of 70 W and an Ar pressure of 0.3 Pa. The distance between target and substrate was 9 cm, corresponding to the ballistic regime [3]. $Fe_{72}Ga_{28}$ films with a thickness of 30 nm and 250 nm, hereafter denoted as thin and thick, were deposited on top of Mo buffers (20 nm) sputtered at 90 W an 0.3 Pa of Ar pressure. To control the thickness of the samples we have firstly established the growth rate by employing test samples whose thickness was ex-situ measured by means of an Alphastep profiler. Then, we adjusted the growth time to obtain samples with the expected thickness. $Fe_{72}Ga_{28}$ films were finally capped with a 20 nm thick Mo layer deposited in the same way as the buffers. XRD in the Bragg-Brentano configuration was performed in a Philips X'Pert MPD using the Cu K_α wavelength (1.54056 Å). The composition of the samples was determined by means of the Energy Dispersive X-ray Spectroscopy (EDS) in a Leica 440 scanning electron

microscope (SEM) operated at 8 kV and 1.5 nA. The magnetic response at room temperature was characterized by vibrating sample magnetometry (VSM) and magneto-optical Kerr effect (MOKE) to analyze bulk and surface magnetism [26-29], respectively. VSM and MOKE measurements were carried out applying in-plane magnetic fields at different angles with respect to an in-plane reference direction taken as the sputtering incidence direction. Measurements at Fe and Ga K-edges were performed in BM25A-SpLine at the European Synchrotron (ESRF) in France. Measurements were performed at room temperature and ambient conditions in fluorescence yield mode. Quality spectra were acquired upon photoelectron wavenumber of 15 $Å^{-1}$ in both edges. The extended X-ray fine structure (EXAFS) region starts after the absorption edge and comprises information about the photoelectron interacting with the local environment of the scattering atom. EXAFS measurements were reduced by standard procedures and fittings were carried out in both *r*- and *k*-spaces [30] using theoretical path functions created with FEFF8.4 [31].

3. Experimental results and discussion

The composition of the layers is $Fe_{72}Ga_{28}$ as in previous films deposited under the same growth conditions in terms of growth power, Ar pressure, and flow regime [3]. When performing compositional maps in the SEM microscope by means of EDS, Fe and Ga appear uniformly distributed within the resolution of the technique. The layers exhibit the Fe-bcc structure typically observed in these alloys [3, 32] with a main diffraction peak related to the (110) reflection (Fig.1). Actually, both Mo and Fe-Ga layers exhibit this (110) as the main diffraction peak. This <110> texture is generally obtained in sputtered Fe-Ga layers because this growth technique generally promotes the stacking of the most dense planes that in bcc structure correspond to (110) planes [33]. The same can be said about Mo, because it also has a bcc structure. From the (110) peak of Fe-Ga, we have calculated a lattice parameter of 2.90 Å for both thicknesses in agreement with reported values [3, 21, 32]. This can also indicate that on average, the strain in the layers can be taken as negligible, or at least, the same in the two studied samples. In general terms, layers can be taken as polycrystalline with evidences of <110> texture, clearer in the thick case.

As shown by bulk and surface magnetic measurements (Figure 2), the thick layer exhibits a clear uniaxial IPMA in the reference direction in agreement with previous

works [3, 34]. For the thin layer, VSM and MOKE loops show no preferential direction revealing in-plane magnetic isotropy. In general, layers with a reduced dimension have a different coercivity than bulk-like systems [1, 35]. The surfaces of thin layers are of increasing importance as the thickness is reduced acting as pinning points for the wall movement and domain nucleation. Therefore, coercivity increases as the thickness is reduced [35] as we have experimentally observed in our samples.

Although nanoprecipitates can be formed in $Fe_{100-x}Ga_x$ [3,9,20], they are not detectable by long-range structural techniques as XRD. Thus, XAFS, as a local structure probe, seems much more appropriate to unveil the whole structural picture [3, 14]. In low dimensional systems, the measurement of linear dichroism in XAFS (LD-XAFS) is an effective way to determine the existence of structural anisotropy from the local point of view [36-37]. This can be performed by analyzing the XAFS signal at two geometries applying a linearly polarized X-ray beam. We can define θ as the angle between the electric field ($\vec{E}$) vector (direction of the X-ray beam) and the normal to the sample surface. Because the beam is linearly polarized in the horizontal plane [38-39], and the photoelectron dispersion has a $\cos^2\theta$ distribution, the XAFS signal becomes sensitive to the structural anisotropy. In brief, for an atomic-scale system with any source of structural anisotropy, we can describe the absorption coefficient (μ^{tot}(E, θ)) as a sum of two contributions, one isotropic, μ^{isot} (E), and another anisotropic, μ^{anisot} (E):

$$\mu^{tot}(E,\theta) = \mu^{isot}(E) + \mu^{anisot}(E) f(\theta) \qquad \text{Eq.1}$$

The function $f(\theta)$ contains the angular dependency of the anisotropy contribution to the total absorption. The absorption coefficient can be rewritten following Dau *et al*. [36]:

$$\mu^{tot}(E,\theta) = \mu^{isot}(E) + \mu^{anisot}(E) I^{ord}(3cos^2\theta - 1) \qquad \text{Eq.2}$$

where the phenomenological parameter, I^{ord}, accounts for the angular distribution of the scattering centers respect to the normal of the sample [40]. I^{ord} is zero for a completely isotropic medium and 1 for a perfectly anisotropic, therefore accounting for the structural anisotropy. It is also useful to get an expression where the experimental number of atomic neighbors (N_{ap}) obtained from EXAFS can be related to the structural anisotropy and to the polarization of the beam respect to the surface:

$$N_{ap} = N\left[1 - \tfrac{1}{2} I^{ord}(3cos^2\theta - 1)\right] \qquad \text{Eq.3}$$

where N is the crystallographic number of neighbors. We performed polarized-XAFS by choosing the angle between the incidence beam direction and the sample plane at two polarization angles, 10° (namely grazing incidence, GI) and 80° (namely normal incidence, NI). Similar investigations have been conducted in amorphous bulk $TbFe_2$ alloys by Harris *et al*. [18-19] and recently by Pascarelli *et al*. [14] although applying different methodologies.

The Fourier transform of the EXAFS signal of Fe and Ga-K edges are represented as a function of the scattering distance from the scattered atom (fig.3 a&b). The polarization dependent signal at the Fe K-edge shows noticeable differences for the thick layer but subtle changes for the thin one. In the case of the Ga K-edge, the amplitude of the first neighbor signal seems equivalent for both polarizations. Semi-quantitative information about the anisotropy was obtained by fitting the EXAFS signal using the average atomic coordination as one of the fitting parameters (table I). Following eq.3, N_{ap} is related to the structural anisotropy through I^{ord}. With this model, the anisotropy inferred from the Fe K-edge data is significantly higher for the thick than for the thin case, which is albeit not nominally zero. We can take this anisotropy in the Fe K-edge as the first evidence of a distortion of the bcc cubic structure in the sample plane in comparison to the out of plane direction. However, it seems there is not such an evident out-of-plane anisotropy or at least, it cannot be detected by EXAFS, in the Ga K-edge. The NI and GI spectra are practically overlapped being the I^{ord} values low for thick and close to zero for the thin layer.

We have also analyzed the near the edge XAFS (NEXAFS) of the Fe and Ga K-edges in the normal and grazing incidences (fig.3 c&d). NEXAFS comprises the region around the absorption edge, being very sensitive to the electronic structure, and local geometry of the scattering atom. However, usually NEXAFS only provides qualitative information and its quantification can become struggling. The main differences can be observed in the edge and white line (the region just after the absorption edge, normally comprising one or more features). Regarding the Fe spectra of the thick film, the main spectral distortions are related to the increase of the pre-peak shoulder intensity and the damping of the white line (opposite to the effect of self-absorption) in the GI polarization. Fe-oxides usually have very intense white lines with a shift in energy and their absorption edges do not present a shoulder but a pre-peak. Therefore, we have ruled out a possible contribution of an oxide layer to the GI because the effect would be contrary to the observed. The pre-edge shoulder in 3d transition metals is related to

dipole forbidden 1s→3d transitions when there exists a partial hybridization of the electronic levels 4p-3d. This is usually caused by scattering atoms placed in a non-centrosymmetric site and, therefore, it is sensitive to anisotropy. By EXAFS, almost no traces of structural anisotropy have been detected in Ga compared to the Fe K-edge. Nevertheless, NEXAFS is much more sensitive to local geometry distortions being possible to observe the structural anisotropy related to Ga (fig. 3 d). A dichroic signal appears in the Ga K-edge for both thicknesses, although it is larger in the thick sample. In this latter sample the dichroic signal presents a double feature, a negative peak followed by a maximum, whereas it only exhibits the negative peak in the thin one (inset: fig. 3d). In the Fe K-edge, a dichroic signal exhibiting a negative peak followed by a maximum is only observed in the thick sample (inset: fig. 3c).

In the local range, the preferential atomic alignment in the sample plane has been determined by performing in-plane angle-dependent polarized-XAFS. We take as the reference axis in the sample plane the sputtering beam direction. The azimuthal angle (α) subtended by the *E*-vector respect to the reference axis was varied being the incidence angle of the beam about 15° respect to the substrate normal. XAFS results for the Fe K-edge presented in figure 4 a&b, and Table 2 show a progressive increase of the Fe coordination as α increases. This effect is clear in the thick layer, while it seems to saturate for angles above 45° in the thin layer. The dependence of the Ga coordination follows the same behavior in the thin layer, but in the thick case N_{ap} is maximum at the sputtering beam direction.

The variance of the shell radius (σ^2) accounts for the atom-to-atom correlative variance of the atomic shell distance, which has a static (atomic disorder) and a dynamic (thermal disorder) contributions. When comparing different polarization orientations within the sample plane it has been found a maximum in the σ^2 of the Ga first shell that coincides with the anisotropy axis direction for the thick film (Table 2). In the thin layer on the contrary there is not a significant modification of this parameter (Table 2). In the Fe K-edge of the two samples, there is a difference of more than 50 % for the σ^2 in the NI respect to the GI (Table 1). In contrast, σ^2 values are almost the same for Ga in that case. Assuming the thermal disorder is the same for all the cases, differences should be due to the static contribution. Cao and coworkers found signatures of precipitation of ordered phases within the regular A2 bcc matrix in $Fe_{100-x}Ga_x$ (x ~ 25 at. %) [9]. They suggested these phases to be distorted cubic aggregates close to tetragonal symmetry.

Those previous results are consistent with our observations that indicate a distortion in the sample plane in the direction of the sputtering beam direction.

The intrinsic uncertainty on the calculation of shell coordination by EXAFS limits the precision on the determination of these values when variations are subtle. Nevertheless, NEXAFS is much more sensitive and it can be used to complete the analysis. In the Fe K-edge, the angular-dependent difference spectra that is the dichroic signal measured in the in-plane experiments only show clear features for the thin layer (inset: fig.4 c). Remarkably, the magnitude of these features is significantly smaller than measured in NI vs. GI experiments. The in-plane Ga K-edge NEXAFS shows evident features in the signal obtained when subtracted in-plane measurements recorded in the sputtering beam direction and perpendicular to it (inset: fig. 4d). Both thick and thin layers, present the negative peak at the same X-ray photon energy although with a weaker intensity than in the LD-XAFS experiments. It is not observed any trace of the second spectral feature, the maximum located at higher energies, present in the LD-XAFS.

In order to identify the structural causes which promote the spectral features of the LD-XAFS (insets: fig. 3 c&d) and the in-plane difference spectra obtained varying the azimuthal angle (insets: fig. 4 c&d), *ab initio* calculations on different Fe-Ga clusters were performed [14]. First, we have constructed a B2 atomic cluster of 3 Å (Ga in the central position) comprising the first atomic shell (8 Fe atoms) considering a static disorder component of 0.002 $Å^2$ accounting for the natural random orientation. The calculations for a 'native' cluster as well as for a distorted with an atom displacement of 0.02 Å along the [001] direction (about 0.1% of cell distortion) have been performed keeping the cell volume. Subsequently, a larger 4 Å cluster which includes the 6 atoms of the second shell was also considered in the calculations. In this later case, modeling the B2 phase in the Ga content range considered in this work implies the two center atoms of the bcc cells are aligned in the [001] direction, i.e. Ga-pairing appears naturally in the studied Ga concentration.

Our calculations show the negative peak at lower energies in the NEXAFS difference spectra is enhanced in the largest cluster that evidences its correspondence with Ga-pairing (fig.5 top curves).When it is increased the atomic distortions along the [001] direction (0.5, 1 and 5%) in the largest cluster, no much variation in the low-energy negative peak but on the maximum that appears at higher energies is observed (fig.5 bottom curves). Therefore, this second feature should be interpreted as an

indicator of the distortion promoted in the direction in which Ga-pairs are ordered, the [001] direction in this calculations.

The negative peak obtained at low energies in the in-plane subtracted signals, as well as their dependence with the azimuthal angle, evidence Ga-pairing along the sputtering direction in the thick layer (inset: fig.4d). Experimental results for the thin film show some ordering, as indicated by the negative peak when comparing $\alpha = 0°$ and $\alpha = 90°$. However, this ordering is smaller than in the thick sample because the peak is not present in the difference spectra between $\alpha = 0°$ and $\alpha = 45°$. Therefore, we can expect a higher amount of ordered B2 phase in the thick sample. The maximum at higher energies sensitive to the cell distortion is only observed in the thick layer when comparing the in- and out-of-plane local structure of Ga (insets: fig.3 c&d). This fact points to a preferential orientation of the cell distortion in the sample plane of the thick layer.

We have found three important aspects: 1) XRD measurements indicate a preferential alignment of the [001] direction in the sample plane for the thick sample, 2) LD-XAFS shows a higher cell distortion in the sample plane, 3) the difference spectra of the azimuthal measurements point out to a higher Ga-pairing along the sputtering direction contained in the sample plane of that layer. We propose as the cause of the uniaxial IPMA in the thick layer a higher and more ordered segregation of B2 phase with a cell distortion along the [001] direction contained in the sample plane. Subtle evidences of Ga-pairs in the sample plane of the thin layer have also found. However, the absence of both a clear cell distortion and an adequate ordering of the Ga-pairs suggest that the formation of IPMA is also dependent on a large enough amount of distorted B2 phase correctly ordered. It is precisely in the thick layer in which we have found a larger amount of such B2 ordered aggregates as indicated by the larger negative peak found in the in-plane difference signals (fig. 4d) and in the LD-XAFS (fig. 3d). Thus, for low thicknesses in which the surface-to bulk term dominates it seems not favorable the formation of a large enough amount of completely ordered B2 phase being necessary a bulk-like thickness. Therefore, the surface to volume ratio should be the decisive parameter governing this transition.

A crossover to perpendicular magnetic anisotropy (PMA) was reported in $Fe_{100-x}Ga_x$ films with *x* between 14 and 29 at.% deposited by MBE [41]. For layers with a thickness of 36 nm, Barturen *et al*. observed an isotropic in-plane magnetic behavior for

x = 29 in agreement with our work. Above a critical thickness of around 35 nm, stripes domains are formed except for x = 29 at. % that seems to keep its in-plane isotropy. In those highly crystalline <100>-textured samples, Ga-pairs along the growth direction generate the tetragonal distortion related to the PMA in layers with $x \leq 20$ at. % [16]. Our experimental results indicate that, in <110> samples with a Ga content around the second peak of magnetostriction the deposition performed in the ballistic regime in the oblique incidence favors the alignment of Ga along the sputtering direction within the sample plane in which it will be the [001] direction. This Ga alignment distorts the bcc structure in that plane forcing a magnetic anisotropy through a magnetocrystalline interaction when the necessary volume-to-surface ratio is reached.

4. Conclusions

In summary, we have performed a combined magnetic and polarization dependent local structure study on high Ga-content $Fe_{100-x}Ga_x$ films of 30 and 250 nm (namely thin and thick). We have clearly observed a structural anisotropy in the thick sample together with evidences of structures other than bcc, including highly distorted bcc. Evidences of Ga-pairing in the sample plane have been found for both thicknesses. However, the ordering of these pairs along the sputtering direction together with a clear distortion when comparing the sample plane and the out of plane direction have only been found in the thick layer. In this sample, the magnetic anisotropy axis is along the direction of maximum Ga alignment set by the sputtering beam. All the results here presented indicate the distorted bcc phase tends to have the elongated axis within the sample plane in these layers. This implies a correlation between the development of an IPMA and the formation of a structural anisotropy as the layer thickness increases. Therefore, the surface to bulk free energy ratio seems to play a key role in the formation of oriented ordered phases in $Fe_{100-x}Ga_x$ alloys for this Ga content. Although in the literature it is often reported the inverse effect (the decrease of uniaxial magnetic anisotropy with film thickness) often due to an interfacial origin, the experimental results here presented show the existence of new phenomena in $Fe_{100-x}Ga_x$ films.

Acknowledgements. We thank 'CAI Difracción de rayos-X' of UCM for x-ray diffractometry measurements and 'Instituto of Sistemas Optoelectrónicos y Microtecnología' (ISOM) for using its facilities. We also want to thank BM25-Spline, the Spanish CRG at ESRF in Grenoble (France) for providing beamtime. This work has

been financially supported through the project MAT2015-66888-C3-3-R of the Spanish Ministry of Economy and Competitiveness (MINECO/FEDER) and project PR26/16-3B-2 of Santander and Universidad Complutense de Madrid.

Table 1. List of EXAFS parameters and phenomenological anisotropy parameter I^{ord} obtained from fittings of the Normal and grazing incidence measurements.

	Fe K-edge				Ga K-edge			
Thickness	**250 nm**		**30 nm**		**250 nm**		**30 nm**	
Polarization	**NI**	**GI**	**NI**	**GI**	**NI**	**GI**	**NI**	**GI**
N_{ap}	7.6(5)	4.3(5)	6.0(7)	5.5(5)	7.4(8)	6.9(8)	7.2(7)	7.1(8)
ΔE_0 (eV)	-5(1)		-5(1)		-5(1)		-5(1)	
***dR* (Å)**	-0.02 (1)	-0.01 (1)	-0.02 (1)	-0.02 (1)	0.02 (1)	0.02 (1)	0.03 (1)	0.01 (1)
σ^2 (Å^2)	0.0089 (6)	0.0052 (7)	0.0075 (5)	0.0056 (6)	0.0077 (8)	0.0073 (8)	0.0082 (9)	0.0079 (9)
R-coef	0.02	0.03	0.02	0.02	0.02	0.04	0.03	0.03
I^{ord}	0.36(5)		0.09(5)		0.05(9)		0.0(1)	

Table 2. List of EXAFS parameters obtained from fittings of the normal incidence measurements taken at different polarization angles respect the sputtering incidence direction (α).

	Fe K-edge					
thickness	**250 nm**			**30 nm**		
α (°)	**0**	**45**	**90**	**0**	**45**	**90**
N_{ap}	6.6(5)	7.2(5)	7.6(5)	5.6(5)	6.4(5)	6.3(5)
ΔE_0 *(eV)*	-5(1)	-5(1)	-4(1)	-4(1)	-3(1)	-4(1)
***dR* (Å)**	-0.01(1)	-0.01(1)	-0.01(1)	-0.01(1)	-0.01(1)	-0.01(1)
σ^2**(Å)**	0.0074 (4)	0.0080(5)	0.0079(5)	0.0062(5)	0.0077(6)	0.0075(5)
R-coef	0.01	0.02	0.02	0.01	0.01	0.01
	Ga K-edge					
thickness	**250 nm**			**30 nm**		
α (°)	**0**	**45**	**90**	**0**	**45**	**90**
N_{ap}	7.9(5)	7.5(5)	7.3(5)	6.6(5)	6.8(5)	7.2(5)
ΔE_0 *(eV)*	1(1)	2(1)	2(1)	1(1)	1(1)	1(1)
***dR* (Å)**	0.00(1)	0.00(1)	0.00(1)	0.00(1)	0.00(1)	0.00(1)
σ^2**(Å)**	0.0093(6)	0.0087(5)	0.0088(5)	0.0081(4)	0.0082(4)	0.0080(4)
R-coef	0.01	0.01	0.01	0.01	0.01	0.01

Figure captions.

Figure 1. Bragg-Brentano XRD diffraction pattern of each layer. The baseline has been corrected. Curves have been shifted for clarity.

Figure 2. Room temperature VSM and MOKE hysteresis loops measured with an in-plane magnetic field in the reference direction (●) 0° between the magnetic field and the reference direction, and (▲) perpendicular to (90°). (a) $Fe_{72}Ga_{28}$ layer with a thickness of 30 nm. (b) $Fe_{72}Ga_{28}$ layer with a thickness of 250 nm.

Figure 3. Fourier transform of the polarized EXAFS spectra of $Fe_{72}Ga_{28}$ layers at normal incidence (NI) in black and grazing incidence (GI) in gray for the (a) Fe and (b) Ga-K edges; corresponding NEXAFS spectra in the (c) Fe and (d) Ga-K edges The inset in c and d figures corresponds to the difference between the NI and GI spectra, defined as linear dichroism (LD).

Figure 4. Fourier transform of the polarized EXAFS spectra of $Fe_{72}Ga_{28}$ layers at normal incidence with different azimuthal angles respect the magnetic anisotropy axis (coinciding with the sputtering reference direction) for the (a) Fe and (b) Ga-K edges; corresponding NEXAFS spectra in the (c) Fe and (d) Ga-K edges. The inset in c and d figures corresponds to the difference spectra between different azimutal angles (α_i).

Figure 5. Ga K-edge NEXAFS difference spectra obtained from *ab initio* calculations using *ad hoc* B2 Fe-Ga clusters with different size, 3 and 4 Å, and with different distortions along the [001] direction for a cluster of 4 Å.

References

[1] S. Chikazumi and C. D. Graham, Jr., *Physics of Magnetism*, Oxford University Press (1997).

[2] B. D. Cullity and C. D. Graham, Jr., *Introduction to Magnetic Materials*, second edition, Wiley IEEE Press (2008).

[3] A. Muñoz-Noval, A. Ordóñez-Fontes, R. Ranchal, Influence of the sputtering flow regime on the structural properties and magnetic behavior of Fe-Ga thin films (Ga ∼ 30 at.%), Phys. Rev. B 93 (2016) 214408.

[4] D. Bisero, E. Angeli, F. Spizzo, P. Vavassori, F. Ronconi, Coercive field vs. temperature in Fe/Ag nanogranular films. J. Magn. Magn. Mater. 262 (2003) 116–119.

[5] A. E. Clark, J. B. Restorff, M. Wun-Fogle, T. A. Lograsso, D. L. Schlagel, Magnetostrictive Properties of Body-Centered Cubic Fe-Ga and Fe-Ga-Al Alloys, IEEE Trans. Magn. 36 (2000) 3238-3240.

[6] A. E. Clark, M. Wun-fogle, T. A. Lograsso, J. R. Cullen, Effect of Quenching on the Magnetostriction of $Fe_{1-x}Ga_x$ ($0.13 < x < 0.21$), IEEE Trans. Magn. 37 (2001) 2678-2680.

[7] M. Laver, C. Mudivarthi, J. R. Cullen, A. B. Flatau, W.-C. Chen, S. M. Watson, M. Wuttig, Magnetostriction and Magnetic Heterogeneities in Iron-Gallium, Phys. Rev. Lett. 105 (2010) 027202.

[8] M. P. Ruffoni, S. Pascarelli, R. Grössinger, R. S. Turtelli, C. Bormio-Nunes, R. F. Pettifer, Direct Measurement of Intrinsic Atomic Scale Magnetostriction, Phys. Rev. Lett. 101 (2008) 147202.

[9] H. Cao, P. M. Gehring, C. P. Devreugd, J. A. Rodriguez-Rivera, J. Li, D. Viehland, Role of Nanoscale Precipitates on the Enhanced Magnetostriction of Heat-Treated Galfenol ($Fe_{1-x}Ga_x$) Alloys, Phys. Rev. Lett. 102 (2009) 127201.

[10] E. Arenholz, G. van der Laan, A. McClure, Y. Idzerda, Electronic and magnetic structure of Ga_xFe_{1-x} thin films, Phys. Rev. B 82 (2010) 180405.

[11] O. Ikeda, R. Kainuma, I. Ohnuma, K. Fukamichi, K. Ishida, Phase equilibria and stability of ordered b.c.c. phases in the Fe-rich portion of the Fe–Ga system, J. Alloys Compnd. 347 (2002) 198-205.

[12] Q. Xing, Y. Du, R. J. McQueeney, T. A. Lograsso, Structural investigations of Fe–Ga alloys: Phase relations and magnetostrictive behavior, Acta Materialia 56 (2008) 4536-4546.

[13] J. Cullen, P. Zhao, M. Wuttig, Anisotropy of crystalline ferromagnets with defects, J. Appl. Phys. 101 (2007) 123922.

[14] S. Pascarelli, M. P. Ruffoni, R. Sato Turtelli, F. Kubel, R. Grössinger, Local structure in magnetostrictive melt-spun $Fe_{80}Ga_{20}$ alloys, Phys. Rev. B **77** (2008) 184406.

[15] R. Ranchal, S. Fin, D. Bisero, Magnetic microstructures in electrodeposited $Fe_{1-x}Ga_x$ thin films ($15 \leq x \leq 22$ at.%), J. Phys. D 48 (2015) 075001.

[16] S. Fin, R. Tomasello, D. Bisero, M. Marangolo, M. Sacchi, H. Popescu, M. Eddrief, C. Hepburn, G. Finocchio, M. Carpentieri, A. Rettori, M.G. Pini, S. Tacchi, In-plane rotation of magnetic stripe domains in $Fe_{1-x}Ga_x$ thin films, Phys. Rev. B 92 (2015) 224411.

[17] M. Barturen, J. Milano, M. Vasquez-Mansilla, C. Helman, M. A. Barral, A. M. Llois, M. Eddrief, M. Marangolo, Large perpendicular magnetic anisotropy in magnetostrictive $Fe_{1-x}Ga_x$ thin films, Phys. Rev. B 92 (2015) 054418.

[18] V. G. Harris, K. D. Aylesworth, B. N. Das, W. T. Elam, N. C. Koon, Structural origins of magnetic anisotropy in sputtered amorphous Tb-Fe films, Phys. Rev. Lett. 69 (1992) 1939.

[19] Vincent G. Harris, Taras Pokhil, Selective-Resputtering-Induced Perpendicular Magnetic Anisotropy in Amorphous TbFe Films, Phys. Rev. Lett. 87 (2001) 067207.

[20] S. Pascarelli, M. P. Ruffoni, A. Trapananti, O. Mathon, C. Detlefs, M. Pasquale, A. Magni, C. P. Sasso, F. Celegato, E. Olivetti, Y. Joly, D. Givord, 4f charge-density deformation and magnetostrictive bond strain observed in amorphous $TbFe_2$ by x-ray absorption spectroscopy, Phys Rev. B. 81 (2010) 020406.

[21] R. Ranchal, S. Fin, D. Bisero, C. Aroca, Tailoring the magnetic anisotropy and domain patterns of sputtered TbFeGa alloys, J. Alloys Compd. 582 (2014) 839-843.

[22] J. Atulasimha, A. B. Flatau, A review of magnetostrictive iron–gallium alloys, Smart Mater. Struct. 20 (2011) 043001.

[23] A. E. Clark, K. B. Hathaway, M.Wun-Fogle, J. B. Restorff, T. A. Lograsso, V. M. Keppens, G. Petculescu, R. A. Taylor, Extraordinary magnetoelasticity and lattice softening in bcc Fe-Ga alloys, J. Appl. Phys. 93 (2003) 8621-8623.

[24] H. Ahmad, J. Atulasimha, S. Bandyopadhyay, Reversible strain-induced magnetization switching in FeGa nanomagnets: Pathway to a rewritable, non-volatile, non-toggle, extremely low energy straintronic memory, Sci. Reports 5 (2015) 18264.

[25] M. Foerster, F. Macià, N, Statuto, S. Finizio, A. Hernández-Mínguez, S. Lendínez, P. V. Santos, J. Fontcuberta, J. M. Hernàndez, M. Kläui, L. Aballe, Direct imaging of delayed magneto-dynamic modes induced by surface acoustic waves, Nature Comm. 8 (2017) 407.

[26] V. Bonanni, D. Bisero, P.Vavassori, G. Gubbiotti, M. Madami, A.O. Adeyeye, S. Goolaup, N. Singh, T. Ono, C. Spezzani, Shape and thickness effects on the magnetization reversal of Py/Cu/Co nanostructures, J. Magn. Magn. Mater. 321 (2009) 3038-3041.

[27] D. Bisero, P. Cremon, M. Madami, M. Sepioni, S. Tacchi, G. Gubbiotti, G. Carlotti, A.O. Adeyeye, N. Singh, S. Goolaup, Effect of dipolar interaction on the magnetization state of chains of rectangular particles located either head-to-tail or side-by-side, J. Nanopart. Res. 13 (2011) 5691-5698.

[28] M. Sepioni, M. Madami, S. Tacchi, G. Gubbiotti, G. Carlotti, D. Bisero, A.O. Adeyeye, N. Singh, S. Goolaup, Dipolar interaction in dense chains of submicrometric rectangular dots, J. Phys.: Conf. Ser. 200 (2010) 072089.

[29] The light penetration depth, and hence, the probe depth is around 30 nm (He-Ne laser with a wavelength of 632 nm).

[30] B. Ravel, M. Newville, ATHENA, ARTEMIS, HEPHAESTUS: data analysis for X-ray absorption spectroscopy using IFEFFIT, Journal of Synchrotron Radiation 12 (2005) 537-541.

[31] A. L. Ankudinov, B. Ravel, J. J. Rehr, S. D. Conradson, Real-space multiple-scattering calculation and interpretation of x-ray-absorption near-edge structure, Phys. Rev. B 58 (1998) 7565.

[32] R. A. Dunlap, N. C. Deschamps, R. E. Mar, S. P. Farrell, Mössbauer effect studies of $Fe_{100-x}Ga_x$ films prepared by combinatorial methods, J. Phys.: Condens. Matter 18 (2006) 4907-4920.

[33] E. du Trémolet de Lacheisserie. Magnétisme. EDP Sciences (2000).

[34] M. Maicas, R. Ranchal, C. Aroca, P. Sánchez, E. López, Magnetic properties of permalloy multilayers with alternating perpendicular anisotropies, Eur. Phys. J. B 62 (2008) 267-270.

[35] G. C. Hadjipanayis (ed.). *Magnetic Hysteresis in Novel Magnetic Materials*, (1997) Kluver Academic Publishers.

[36] J Dittmer, H. Dau, Theory of the Linear Dichroism in the Extended X-ray Absorption Fine Structure (EXAFS) of Partially Vectorially Ordered Systems, J. Phys Chem. B. 102 (1998) 8196-8200.

[37] Characterizarion of Semiconductors Heterostructures and Nanostructures, Second Edition. Editors: Lamberti C and Agostini G. Elsevier Science, 09 April 2013. ISBN: 9780444595515.

[38] G. R. Castro, Optical design of the general-purpose Spanish X-ray beamline for absorption and diffraction, J. Synchrotron Rad. 5 (1998) 657-660; J. R. Rubio-Zuazo, G.R. Castro, Hard X-ray photoelectron spectroscopy (HAXPES) ($\leqslant$15 keV) at SpLine, the Spanish CRG beamline at the ESRF, Nuclear Instruments and Methods in Physics Research Section A. 547 (2005) 64-72.

[39] C. Brouder, Angular dependence of X-ray absorption spectra, J. Phys.: Condens. Matter 2 (1990) 701.

[40] A. Manceau, M. L. Schlegel, Texture effect on polarized EXAFS amplitude, Phys. Chem. Minerals 28 (2201) 5256.

[41] M. Barturen, B. Rache Salles, P. Schio, J. Milano, A. Butera, S. Bustingorry, C. Ramos, A. J. A. de Oliveira, M. Eddrief, E. Lacaze, F. Gendron, V. H. Etgens, M. Marangolo, Crossover to striped magnetic domains in $Fe_{1-x}Ga_x$ magnetostrictive thin films, Appl. Phys. Lett. 101 (2012) 092404.

Figure 1

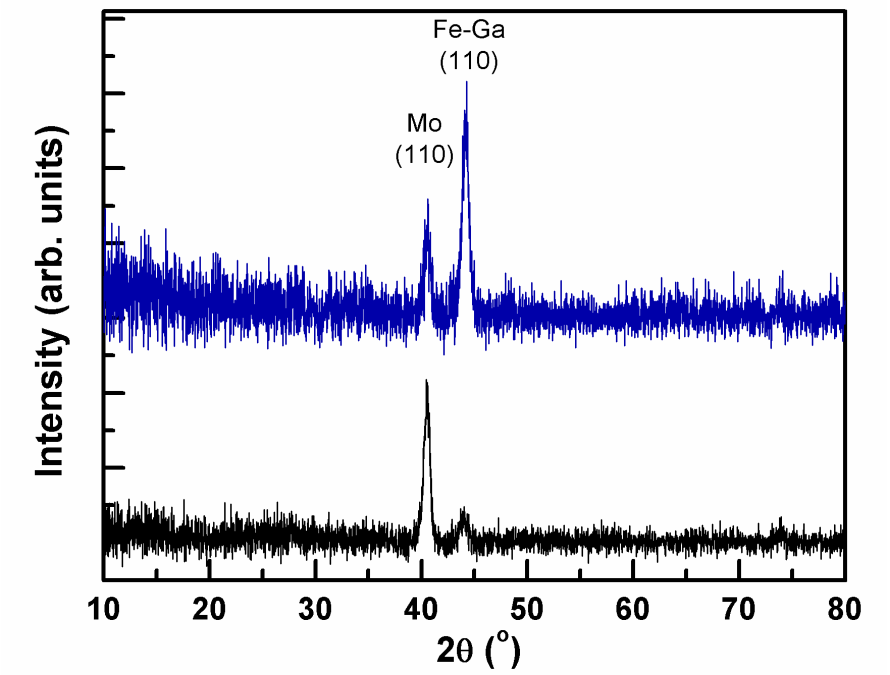

Figure 2

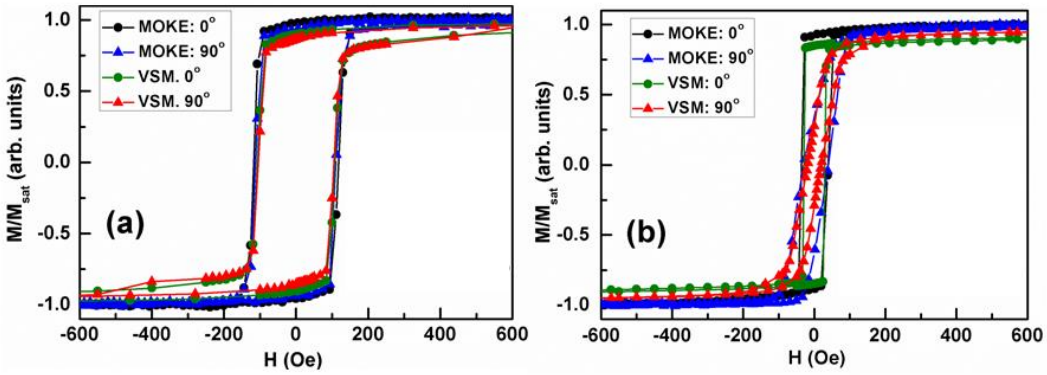
MOKE: 0°
MOKE: 90°
VSM. 0°
VSM. 90°
(a)
M/M_sat (arb. units)
H (Oe)
MOKE: 0°
MOKE: 90°
VSM: 0°
VSM: 90°
(b)
M/M_sat (arb. units)
H (Oe)

Figure 3

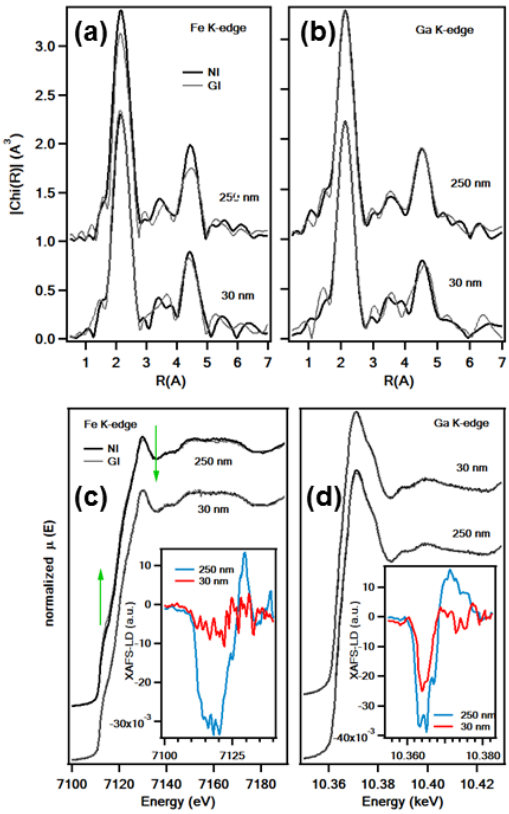
(a)
Fe K-edge
NI
GI
250 nm
30 nm
|Chi(R)| (A^3)
R(A)
(b)
Ga K-edge
250 nm
30 nm
R(A)
(c)
Fe K-edge
NI
GI
250 nm
30 nm
normalized μ (E)
XAFS-LD (a.u.)
250 nm
30 nm
-30x10^{-3}
Energy (eV)
(d)
Ga K-edge
30 nm
250 nm
XAFS-LD (a.u.)
250 nm
30 nm
-40x10^{-3}
Energy (keV)

Figure 4

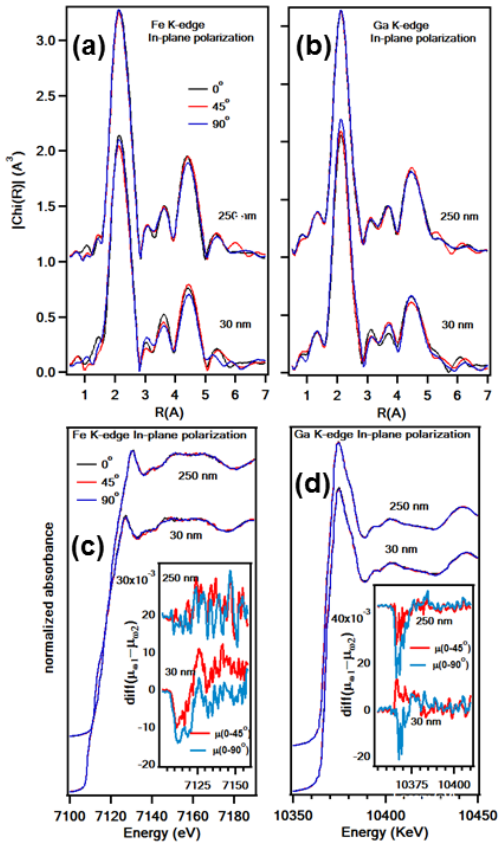
(a)
Fe K-edge
In-plane polarization
0°
45°
90°
250 nm
30 nm
|Chi(R)| (A^-3)
R(A)
(b)
Ga K-edge
In-plane polarization
250 nm
30 nm
R(A)
(c)
Fe K-edge In-plane polarization
0°
45°
90°
250 nm
30 nm
30x10^-3
250 nm
30 nm
μ(0-45°)
μ(0-90°)
normalized absorbance
Energy (eV)
(d)
Ga K-edge In-plane polarization
250 nm
30 nm
40x10^-3
250 nm
μ(0-45°)
μ(0-90°)
30 nm
Energy (KeV)

Figure 5

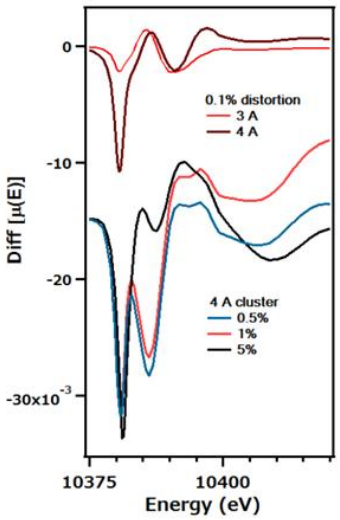
0
-10
-20
-30x10^-3
Diff [μ(E)]
0.1% distortion
3 A
4 A
4 A cluster
0.5%
1%
5%
10375
10400
Energy (eV)